Supplement of Atmos. Chem. Phys., 21, 16479–16497, 2021
https://doi.org/10.5194/acp-21-16479-2021-supplement

Supplement of

Examining the competing effects of contemporary land management vs. land cover changes on global air quality

Anthony Y. H. Wong and Jeffrey A. Geddes

Correspondence to: Jeffrey A. Geddes (jgeddes@bu.edu)

Text S1. Here we provide our reasoning for considering changes in displacement height (*d*) as negligibly small compared to changes in roughness length (z_o). Equation S1 demonstrates how aerodynamic resistance (R_a) is typically calculated in land surface exchange scheme:

$$R_a = \frac{1}{\kappa u_*}\left(\ln\left(\frac{z-d}{z_0}\right) - \Psi\left(\frac{z-d}{L}\right) + \Psi\left(\frac{z_0}{L}\right)\right) \text{(S1)}$$

where κ is von Kármán constant, u_* is friction velocity (m s^{-1}), *L* is Obukhov Length (*L*), *z* is altitude, z_o is roughness length, and *d* is displacement height (m) (Foken, 2006). Since the middle of the first vertical grid of GEOS-Chem (*z*) is around 60 – 70 meters (http://wiki.seas.harvard.edu/geos-chem/index.php/GEOS-Chem_vertical_grids), which is significantly larger than *d* such that $z - d \approx z$ under most conditions, the changes in *d* are expected to be less important than the changes in z_0.

Text S2. The population-weighted averaged changes surface O_3 (ppb) or $PM_{2.5}$ (μg m^{-3}) ($\Delta[X]_{\text{pop\_weighted, Y}}$) for region Y is calculated as follow:

$$\Delta[X]_{\text{pop\_weighted,Y}} = \frac{\sum_i^{gridcells\ in\ \text{Y}} \Delta[X]_i Pop_i}{\sum_i^{gridcells\ in\ \text{Y}} Pop_i} \text{(S2)}$$

where $\Delta[X]_i$ is changes in surface concentration of concerned chemical species, and Pop_i is the population count for individual gridcell i. The global gridded population is from the fourth version of The Gridded Population of the World (GPWv4) (CIESIN, 2018), and remapped to match the resolution of GEOS-Chem output.

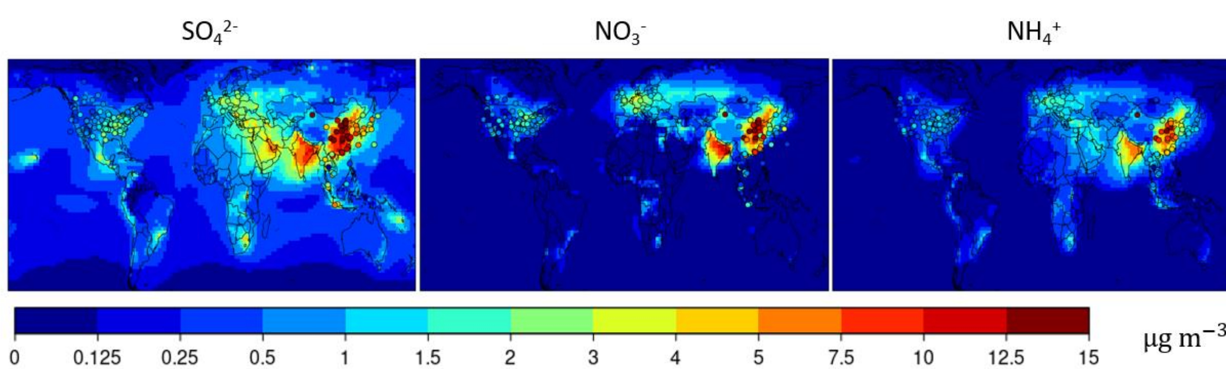

Fig. S1 Modelled annual surface concentration of SO_4^{2-}, NO_3^{2-} and NH_4^+ aerosol for 2014. Filled circles indicate measured annual means for 2014 compiled from Air Quality System (AQS) of Environmental Protection Department (EPD) for United States (US), National Atmospheric Chemistry (NAtChem) database for Canada, European Monitoring and Evaluation Programme (EMEP) for Europe, Acid Deposition Monitoring Network in East Asia (EANET) for eastern Asia, and Geng et al. (2017) for China. The data from AQS, NAtChem, EMEP and EANET.

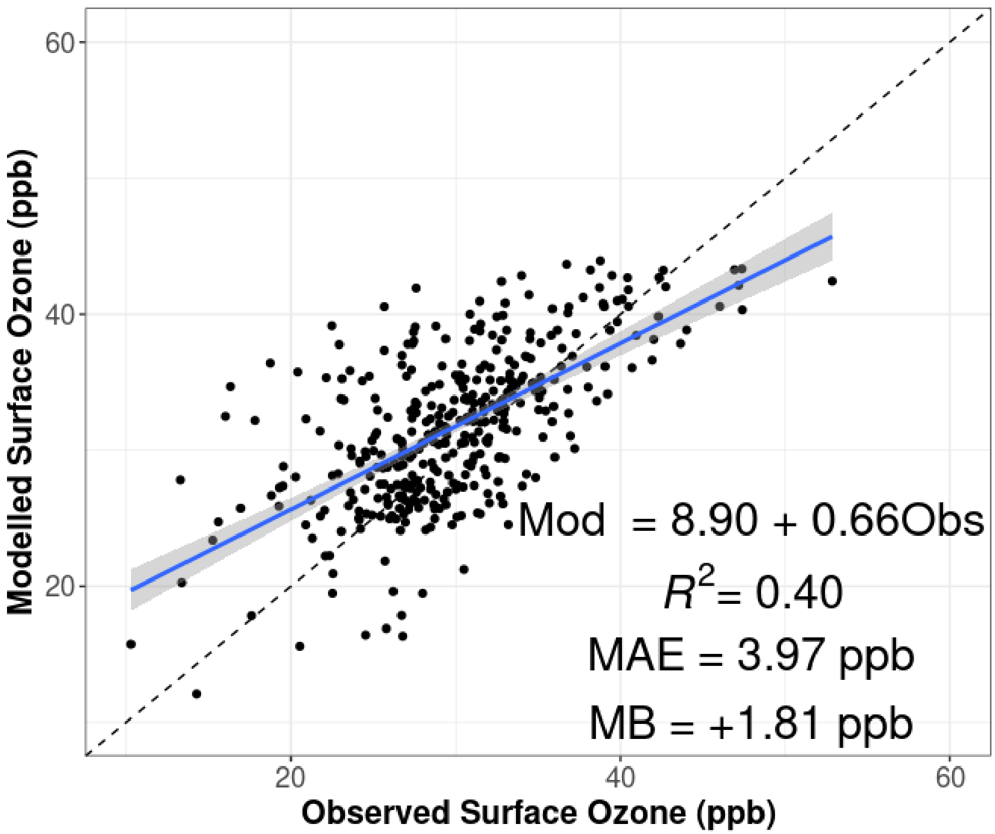

Fig. S2 Comparison between mean modelled and observed surface ozone compiled by Sofen et al. (2016) at 2014. MAE and MB represents the mean absolute error and mean bias, respectively.

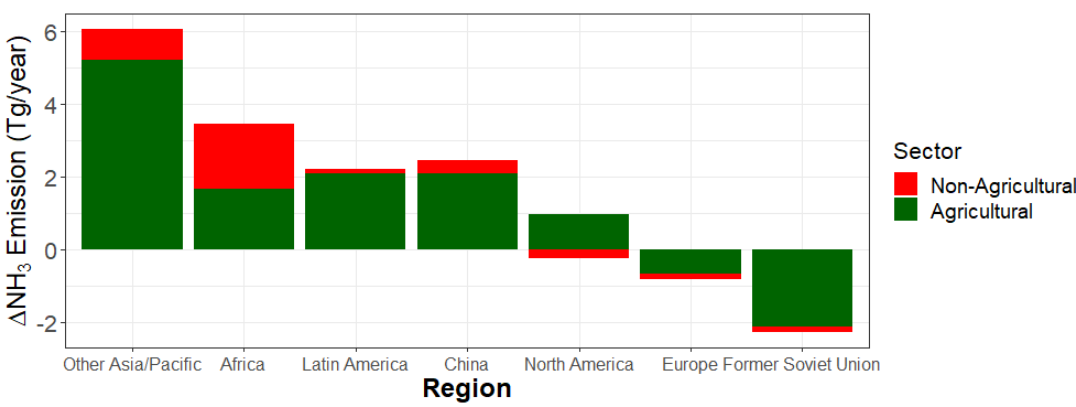

Figure S3. Regionally changes (2014 – 1992) in agricultural and non-agricultural NH_3 emissions from CEDS.

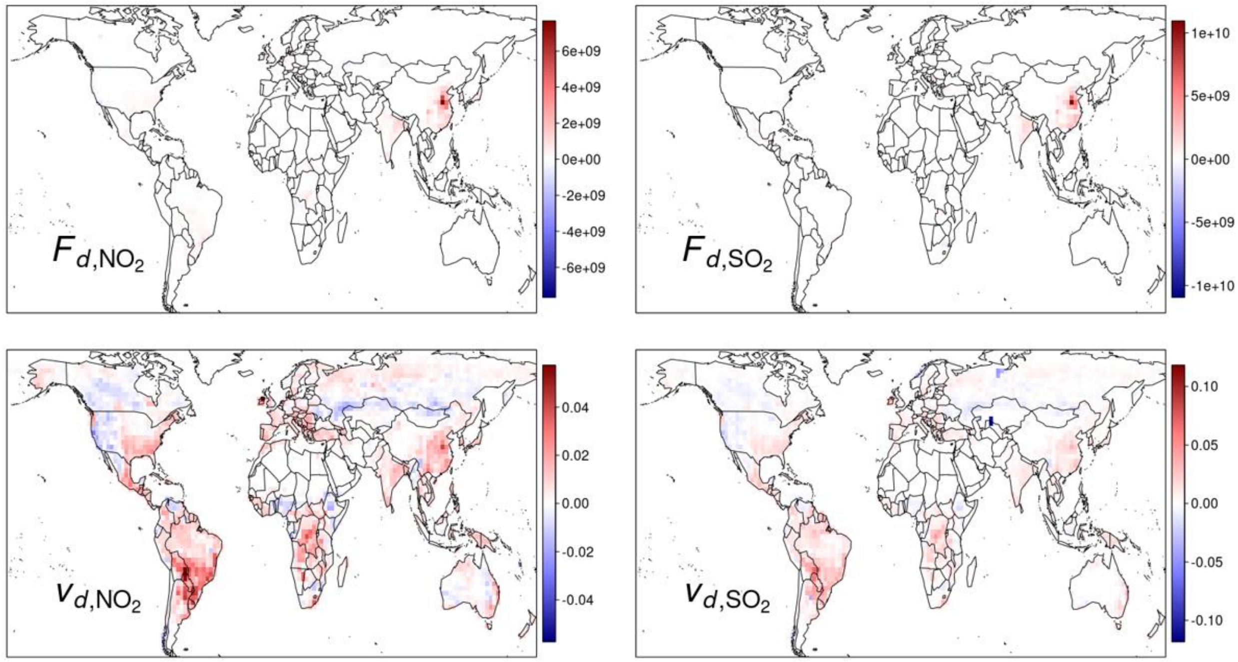

Figure S4. LULCC-induced changes in annual mean dry deposition (v_d) velocity (cm s^{-1}) and flux (F_d) (molec cm^{-2} s^{-1}) in of NO_2 and SO_2.

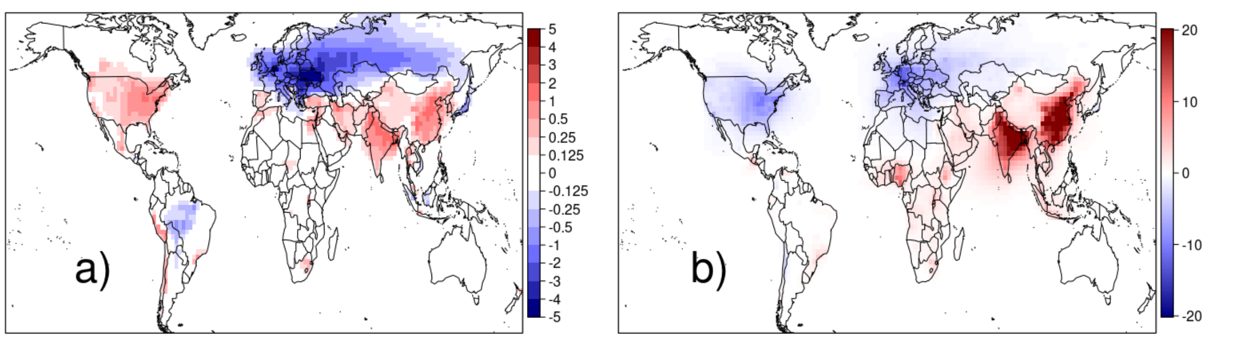

Figure S5. Change in annual mean $PM_{2.5}$ (in µg m^{-3}) due to a) LULCC and changes in agricultural emissions at 1992 anthropogenic emissions background (simulation 5 – simulation 1), and b) anthropogenic emission changes (including agricultural emissions) (simulation 4 – simulation 5).

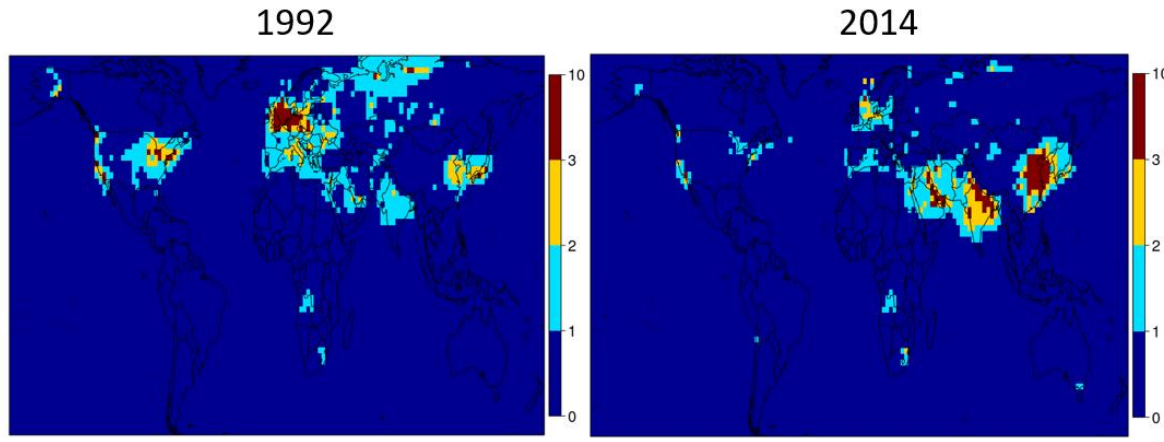

Figure S6. Annual mean surface HNO_3/H_2O_2 ratio under 1992 and 2014 anthropogenic emission background.

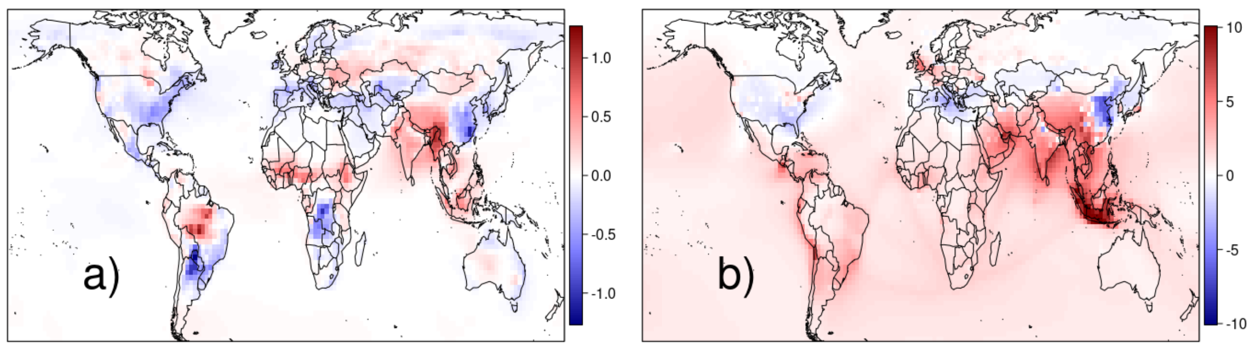

Figure S7. Change in annual mean surface O_3 (in ppbv) due to a) LULCC and changes in agricultural emissions at 1992 anthropogenic emissions background (simulation 5 – simulation 1), and b) anthropogenic emissions changes (including agricultural emissions) (simulation 4 – simulation 5).

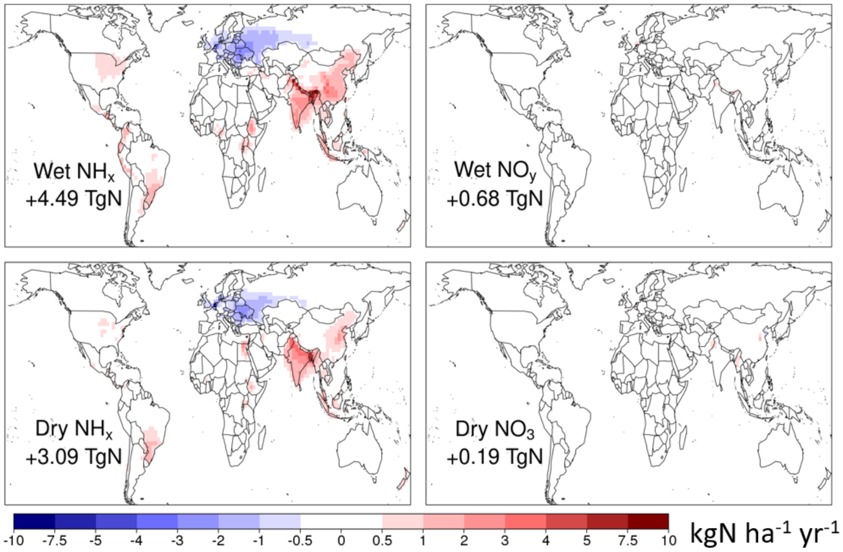

Figure S8. Contribution of different pathways (wet vs dry, reduced (NH_x) vs oxidized (NO_y)) to the changes in total nitrogen deposition. $NH_x \equiv NH_3 + NH_4$ and $NO_y \equiv NO + NO_2$ + HONO + organic nitrates + aerosol nitrate.

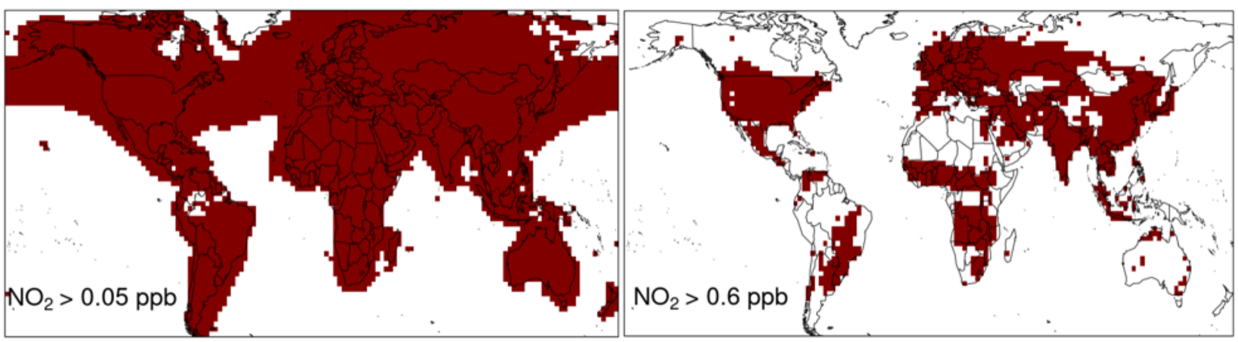

Figure S9. Grid cells (denoted in red) with annual mean NO_2 concentration exceeding 0.05 and 0.6 ppb.

Region	Species	Mod	Obs	Mod/Obs
US	SO_4^{2-}	0.88	1.27	0.70
	NO_3^-	0.77	0.93	0.83
	NH_4^+	0.54	0.69	0.79
Canada	SO_4^{2-}	0.78	0.92	0.85
	NO_3^-	0.84	0.44	1.92
	NH_4^+	0.52	0.36	1.46
Europe	SO_4^{2-}	1.84	2.08	0.88
	NO_3^-	1.67	1.51	1.10
	NH_4^+	1.16	1.11	1.05
China	SO_4^{2-}	8.53	18.93	0.45
	NO_3^-	6.16	10.15	0.61
	NH_4^+	4.83	7.61	0.64
EANET	SO_4^{2-}	2.33	3.64	0.64
	NO_3^-	1.09	1.31	0.84
	NH_4^+	1.15	1.01	1.14

Table S1. Comparison between modelled and observed annual average surface sulphate, nitrate and ammonium aerosol mass (in $\mu g\ m^{-3}$) over different region/observational network. Measurements are compiled from Air Quality System (AQS) of Environmental Protection Department (EPD) for United States (US), National Atmospheric Chemistry (NAtChem) database for Canada, European Monitoring and Evaluation Programme (EMEP) for Europe, Acid Deposition Monitoring Network in East Asia (EANET) for eastern Asia, and Geng et al. (2017) for China. The data from AQS, NAtChem, EMEP and EANET are collect in 2014.

Region	Countries included
Former Soviet Union (FSU)	Armenia, Azerbaijan, Belarus, Georgia, Kazakhstan, Kyrgyzstan, Moldova, Russia, Tajikistan, Turkmenistan, Ukraine, Uzbekistan
Western Europe (WEU)	Austria, Belgium, Switzerland, Germany, Denmark, Spain, Finland, France, United Kingdom, Greece, Ireland, Iceland, Italy, Luxembourg, Netherlands, Norway, Portugal, Sweden
Central and eastern Europe (CEU)	Albania, Bulgaria, Bosnia and Herzegovina, Cyprus, Czechia, Estonia, Croatia, Hungary, Kosovo, Lithuania, Latvia, Montenegro, Poland, Romania, Serbia, Slovakia, Slovenia
China	China
South Asia (SAs)	Afghanistan, Bangladesh, Bhutan, India, Sri Lanka, Nepal, Pakistan
Middle East (ME)	United Arab Emirates, Egypt, Iran, Iraq, Israel, Kuwait, Lebanon, Oman, Qatar, Saudi Arabia, Syria, Turkey, West Bank, Yemen
Southeast Asia (SEA)	Brunei, Indonesia, Cambodia, Laos, Myanmar, Malaysia, Philippines, Thailand, Vietnam

Japan and Korea (JK)	Japan, South Korea, North Korea
Australasia (Aus)	Australia, Fiji, New Caledonia, New Zealand, Papua New Guinea, Solomon Islands, Vanuatu
North America (NAm)	Canada, United States
Central America (CAm)	Belize, Costa Rica, Cuba, Guatemala, Honduras, Haiti, Jamaica, Mexico, Nicaragua, Panama, Puerto Rico, El Salvador, Trinidad and Tobago
South America (SAm)	Argentina, Bolivia, Brazil, Chile, Colombia, Ecuador, Guyana, Peru, Paraguay, Suriname, Uruguay, Venezuela, French Guiana
Northern Africa (NAf)	Algeria, Libya, Morocco, Tunisia
Western Africa (WAf)	Benin, Burkina Faso, Ivory Coast, Cameroon, Gabon, Ghana, Guinea, Gambia, Guinea Bissau, Liberia, Mali, Mauritania, Niger, Nigeria, Senegal, Sierra Leone, Chad, Togo
Southern Africa (SAf)	Angola, Botswana, Lesotho, Mozambique, Malawi, Namibia, Swaziland, South Africa, Zambia, Zimbabwe
Eastern Africa (EAf)	Burundi, Djibouti, Eritrea, Ethiopia, Kenya, Madagascar, Rwanda, Sudan, Somaliland, Somalia, Uganda

Table S2. Definition of regions.

Region†	$\Delta PM_{2.5(LULCC+agr\_emis,1992)}$	$\Delta O_{3(LULCC+agr\_emis,1992)}$
FSU	-0.69 (-1.95)	-
WEU	-0.49 (-1.24)	-
CEU	-2.03 (-2.22)	-
China	+0.34 (+0.75)	+0.09 (-0.21)
SAs	+0.55 (+0.82)	+0.26 (+0.25)
ME	+0.20 (+0.33)	-
SEA	+0.21 (+0.17)	+0.32 (+0.26)
JK	-0.08 (-0.23)	-
NAm	+0.15 (+0.56)	-0.05 (-0.21)
CAm	+0.10 (+0.22)	-
WAf	-	+0.20 (+0.30)
EAf	-	+0.16 (+0.27)
Global	-0.08 (+0.23)	+0.01 (+0.03)

Table S3. Changes in area averaged, and population-weighted (in parentheses), annual mean surface $PM_{2.5}$ ($\Delta PM_{2.5(LULCC+agr\_emis,1992)}$, in µg m^{-3}) and O_3 ($\Delta O_{3(LULCC+agr\_emis,1992)}$, in ppbv) concentrations due to combined effects of LULCC and agricultural emission evaluated under 1992 anthropogenic emission background. Results only from regions with area- or population-weighted average $\Delta PM_{2.5(LULCC+agr\_emis,1992)} > 0.2$ µg m^{-3} or $\Delta O_{3(LULCC+agr\_emis,1992)} > 0.2$ ppbv are shown.

†**The definitions and abbreviations of all regions can be found in Table S2.**

Reference

Foken, T. (2006). 50 years of the Monin-Obukhov similarity theory. In *Boundary-Layer Meteorology* (Vol. 119, Issue 3, pp. 431–447). https://doi.org/10.1007/s10546-006-9048-6

Geng, G., Zhang, Q., Tong, D., Li, M., Zheng, Y., Wang, S., & He, K. (2017). Chemical composition of ambient PM2. 5 over China and relationship to precursor emissions during 2005-2012. In *Atmospheric Chemistry and Physics* (Vol. 17, Issue 14, pp. 9187–9203). https://doi.org/10.5194/acp-17-9187-2017

Sofen, E. D., Bowdalo, D., Evans, M. J., Apadula, F., Bonasoni, P., Cupeiro, M., Ellul, R., Galbally, I. E., Girgzdiene, R., Luppo, S., Mimouni, M., Nahas, A. C., Saliba, M., & Tørseth, K. (2016). Gridded global surface ozone metrics for atmospheric chemistry model evaluation. *Earth System Science Data*. https://doi.org/10.5194/essd-8-41-2016

CIESIN, Center for International Earth Science Information Network, Columbia University (2018). Gridded Population of the World, Version 4 (GPWv4): Population Density Adjusted to Match 2015 Revision UN WPP Country Totals, Revision 11. NASA Socioeconomic Data and Applications Center (SEDAC)